Journal of Hydrology: Regional Studies 19 (2018) 287–306

Contents lists available at ScienceDirect

Journal of Hydrology: Regional Studies

journal homepage: www.elsevier.com/locate/ejrh

Analysis of rainfall extremes and water yield of Krishna river basin under future climate scenarios

Chanapathi Tirupathi[a], Thatikonda Shashidhar[a,*], Raghavan Srinivasan[b]

[a] Department of Civil Engineering, IIT- Hyderabad, Sangareddy, Kandi, Telangana, 502 285, India
[b] Department of Ecosystem Science and Management, Texas A&M University, 2138, TAMU, College station, TX, 77845, USA

ARTICLE INFO

Keywords:
Climate change
ISMR
Krishna river basin
Extreme rainfall events
SWAT model

ABSTRACT

Study region: Krishna river basin is the second largest river basin in Peninsular India. The basin largely falls under a semi-arid zone, around a central arid zone. One-third of the basin comes under the Deccan traps, with major soil types being black soils, alluvium, red and mixed soils.

Study focus: In the present study, SWAT has been used to investigate the potential impacts of climate change on the water resources of the Krishna basin. The simulations were carried out with the observed, historical, and future climate data of various climate models and the results were evaluated. The calibration and validation of the model was carried out using the SUFI-2 algorithm in SWAT-CUP. Analysis of rainfall extremes and available water resources were determined under future climate scenarios.

New hydrological insights for the region: Extension of monsoon rainfall even up to October, a shift in the maximum amount of long-term mean ISMR and surface runoff, increasing trend of rainfall in the months of October, November and few extreme rainfall events other than monsoon season was observed under future with different climate models. The climate model (CNRM-CM5) projected that 7%, 5% and 25% of the events were falling under excess rainfall (> 25%), extreme rainfall (> 50%) and moderate drought events respectively under RCP 4.5 scenario, as against 17%, 10% and 17% respectively in the case of RCP 8.5 scenario.

1. Introduction

Water plays a vital role in the survival of human beings and other living things. It is an essential commodity for economic growth, development of agriculture activities, and industries. However, it has become a scarce resource because of increasing population and industrialization (Prajnya and Tuppad, 2016). To overcome the future water stress, sustainable water resources management is essential from the regional to national scales (Shrestha and Htut, 2016; Vu et al., 2016). Further, changes in climate events and weather extremes have had a significant impact on natural water resources. Various studies indicate climate extreme events are increasing in the future because of changes in intense rainfall events, and abruptly high and low temperatures (Easterling et al., 2000; Mukherjee et al., 2018). Therefore, the changes in the frequency of extreme weather events such as droughts or floods could affect the water availability, human health, quality of water resources, agricultural production and environmental conditions (Jiang et al., 2007; Karl, 2008; Mishra et al., 2016). Thus, investigating these impacts on the hydrological regime is crucial for mitigating the adverse effects of extreme weather events.

Hydrological models have been used to evaluate the climate change impacts on the hydrological regimes. These tools help to

* Corresponding author. Present address: Department of Civil engineering, IIT-Hyderabad, Sangareddy, Kandi, Telangana, 502 285, India.
E-mail address: shashidhar@iith.ac.in (S. Thatikonda).

https://doi.org/10.1016/j.ejrh.2018.10.004
Received 23 June 2018; Received in revised form 5 October 2018; Accepted 16 October 2018
Available online 28 October 2018

estimate various hydrological parameters such as runoff, evapotranspiration (ET), potential evapotranspiration (PET) and water yield etc., in its regime. Estimation of these parameters and selection of models are crucial for evaluating the impact of present and future climate (Mishra et al., 2008). SWAT model has been selected for quantifying the hydrological parameters under present and future climate at basin scale (Arnell and Reynard, 1996; Devkota and Gyawali, 2015; Fujihara et al., 2008; Gosain et al., 2006, 2011; Guo et al., 2002; Iskender and Sajikumar, 2016; Mishra and Lilhare, 2016; Molina-Navarro et al., 2016; Singh and Gosain, 2012; Yang et al., 2008; Zhang et al., 2006, 2015; Zierl and Bugmann, 2005).

The Krishna river basin, India was selected as study area due to its semi-arid nature, and vulnerability to climate change, owing to the erratic distribution of rainfall along with warmer climatic conditions. Few studies have been conducted to analyse the climate change impact on water resources of the Krishna river basin. However, these studies use the greenhouse gas (GHG) and Special Report on Emissions Scenarios (SRES) scenarios, which carry an enormous uncertainty in the assumption of factors such as economic development, population growth, and developed technology (Soro et al., 2017). For instance, using the GHG scenario, Gosain et al. (2006) concluded the Krishna basin to experience regular or seasonal water-stressed conditions in future, due to a decrease of precipitation and water yield. Kulkarni et al. (2014) projected an increasing trend in annual precipitation, surface runoff, water yield and actual evapotranspiration in future (2041-70), displaying no significant changes in these parameters in the early century (2011-40) using the SRES scenario. In both these studies, a single GCM data was used without any bias correction, while performing calibration at the only one-gauge station. Mishra and Lilhare (2016) projected an increasing trend of water balance components along with rainfall and air temperature in Krishna river basin under future climate scenarios (CMIP5 models with RCP 4.5 and 8.5 scenarios).

Unlike previous studies (Gosain et al., 2006; Kulkarni et al., 2014), emphasizes on climate model selection based on the performance of the model with reference to observed data. In this study, the rainfall extremes under future climate scenarios of the Krishna river basin, India were analysed. Downscaled and bias-corrected climate models with medium (RCP 4.5) and high emission (RCP 8.5) scenarios were used to improve future predictions and the model performance which was carried out by multi gauge calibration.

2. Research methodology

The methodology follows as (1) Selection of climate model; (2) Hydrological modeling of Krishna river basin with multi gauge calibration and validation; 3) Assessment of water resources under present and future climate scenarios with calibrated model; 4) Analysis of simulated hydrological variables along with impact of projected rainfall to understand extreme weather events.

2.1. Study area

The Krishna river basin (13°5′58″ - 19°24′35″N, 73°20′28″- 81°0′43″E) is the second largest river basin in Peninsular India (Fig. 1). It extends over states of Andhra Pradesh, Karnataka, Telangana, and Maharashtra, covering a total geographic area of 2,58,948 km^2,

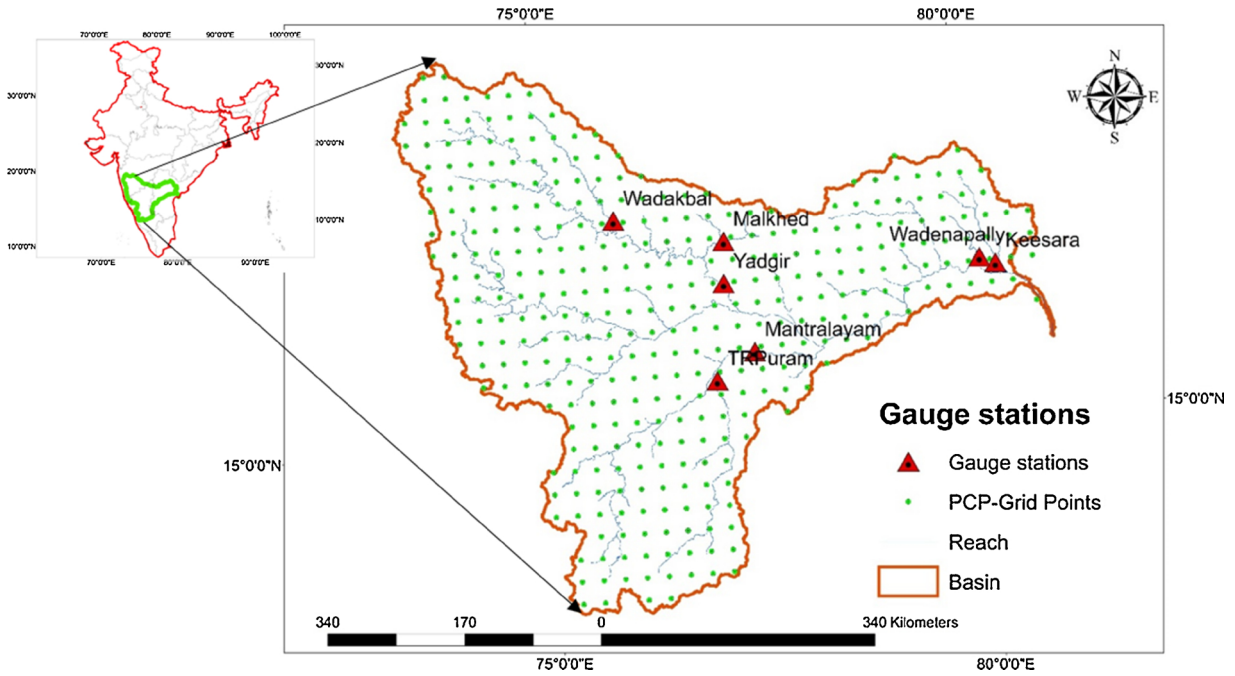

Fig. 1. Location map of Krishna river basin, streams, PCP grid points.

and flows over a length of 1400 km. A major part of this basin lies on basaltic and crystalline rocks, having low yield potentials, while the delta regions have alluvium sediments having high yield potential. The major soil types are black soils, alluvium, red soils, mixed soils, saline and alkaline soils and laterite soils. Most of the area in this basin belongs to a semi-arid region with agricultural land covering about 76% of the total area (NRAA, 2011). The annual average rainfall of the basin is about 780 mm and 90% of it occurs during monsoon (June-October). Some parts of Andhra Pradesh, Karnataka and Maharashtra are drought-prone areas, whereas the delta region is subjected to flooding (http://india-wris.nrsc.gov.in).

2.2. Soil water assessment tool (SWAT)

It is a physically based, semi-distributed, continuous time basin scale model developed to quantify the relative impact of land management practices, climate, and vegetation on water quantity and quality. It is also used to quantify sediment yields, agricultural and chemical yields on large complex watersheds (Arnold et al., 1998; Gosain et al., 2011; Neitsch et al., 2011). Weather data, Digital Elevation Model (DEM), soil, land use/land cover, and slope maps are required as the inputs for model setup, which in turn simulate the water and sediment movement, nitrogen cycle, phosphorus cycle and crop growth at the Hydrologic Response Unit (HRU) level for both, gauged and ungauged catchments. SWAT model uses water balance equation to simulate hydrology of the catchment (Ghoraba, 2015; Prajnya and Tuppad, 2016).

$$SW_t = SW_0 + \sum_{i=1}^{t} (R_{day} - Q_{surf} - E_a - w_{seep} - Q_{gw}) \quad (1)$$

Where SW_0 and SW_t are the initial and final soil water content on day i (mm water) respectively.

t is time (days); R_{day}, Q_{suf}, E_a, W_{seep} and Q_{gw} is the amount of precipitation, surface runoff, evapotranspiration, water entering the vadose zone from the soil profile, and return flow on day i (mm water) respectively.

The present study considered rainfall, surface runoff, evapotranspiration, and water yield as water balance components. Water yield (WYLD) = Surface runoff contribution to streamflow (SURQ) + lateral flow contribution to streamflow (LATQ) + Ground water contribution to streamflow (GWQ)- Total losses (TLOSS) – Pond abstractions. SWAT model was run for a period of 33 years from 1981 to 2013 (including a warm up period of 2 years). SCS curve number method was used to estimate surface runoff from rainfall in the model, based on the properties of land use, soil, and hydrological conditions of the watershed (Arnold et al., 1998;

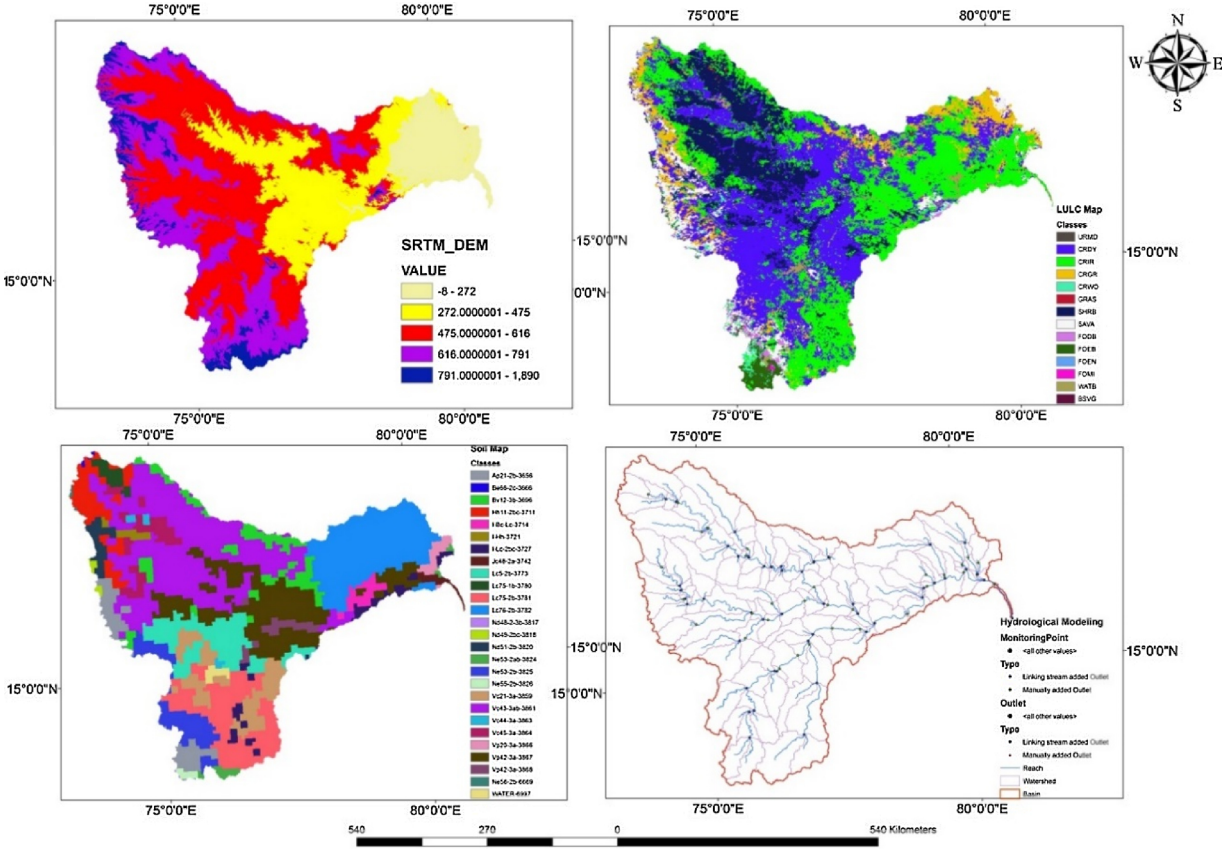

Fig. 2. DEM (90 × 90 SRTM), LU/LC map, Soil map, and Watershed showing streams and outlet points of Krishna river basin.

Ghoraba, 2015). The variable storage method and Priestley-Taylor methods were used for flow routing and estimation of potential evapotranspiration in the model. The model setup is shown in Fig. 2.

2.3. Input data

2.3.1. Geospatial data

The topography details, soil characteristics, and land use/ land cover (LULC) maps were required for the hydrological modeling setup. The topographic details of the study area were provided in SWAT as DEM. Shuttle Radar Topography Mission Digital Elevation Model (SRTM-DEM) of 90 m resolution was used, which was obtained from the CGIAR Consortium for Spatial Information (CGIAR-CSI) (http://srtm.csi.cgiar.org/). The required soil and LULC maps of the study area are obtained from water base (http://www.waterbase.org/) and prepared as per SWAT model (Fig. 2).

2.3.2. Weather data

The rainfall data ($0.25^{\circ} \times 0.25^{\circ}$), and minimum and maximum temperatures ($0.5^{\circ} \times 0.5^{\circ}$) were used as weather inputs for the model, obtained from Indian Meteorological Department (IMD), Pune, India (Pai et al., 2014). The other required data such as solar radiation, wind speed, and relative humidity were autogenerated by the SWAT in build weather generator.

The climate data for the historic (1970–2005) and future scenarios (2006–2100) were obtained from Earth System Grid Federation (ESGF) (https://esg-dn1.nsc.liu.se) i.e., CORDEX-South Asia database. Mishra et al. (2014) reported that, due to low bias and uncertainty, BEST-GCMs may perform better than CORDEX RCMs and their HOST GCMs in hydrological applications which are attributed to intermodal variations. Thus, for using RCMs, bias-correction has to be carried out for regional studies or hydrological applications (Brown et al., 2008; Mishra et al., 2014; Teutschbein and Seibert, 2012). However, in Western Ghat regions, the CORDEX-RCMs may perform better than CMIP5 models because of their ability to resolve orographic and topographic precipitation (Mishra et al., 2014). Since the Krishna river basin receives ample amount of rainfall from western ghat regions (average annual rainfall over 2500 mm) (Gumma et al., 2011), in this study CORDEX- RCMs were used instead of CMIP5 models.

Data from six climate models (ICHES-EC-EARTH, NOAA-GFDL-GFDL-ESM2M, MIROC-MIROC5, NCC-NorESM1-M, IPSL-CM5A-MR and CNRM-CERFACS-CNRM-CM5) were used, comprising of high resolution ($0.5^{\circ} \times 0.5^{\circ}$) climate data with RCP 4.5 and RCP 8.5 scenarios. The RCP 4.5 and 8.5 scenarios stabilize the radiative force at 4.5 and 8.5 W/m^2, based on assumptions of economic activities, population growth, energy sources and social-economic factors. It also includes global, long-term greenhouse gas emissions and land use/land cover (LULC) changes in the global economic framework (Thomson et al., 2011). As a part of mitigation strategy, the expansion of forest is also considered in RCP 4.5.

2.4. Calibration and validation

SWAT-CUP (SWAT-Calibration Uncertainty Programme) was developed for calibration and validation of SWAT model (Abbaspour et al., 2015). To minimize the uncertainty associated with model predictions, the calibration and validation of the model were carried out based on the observed streamflow data, by using the SUFI-2 algorithm in the SWAT-CUP (Abbaspour et al., 2015; Ghoraba, 2015; Yang et al., 2008). The uncertainty and sensitivity analysis were also carried out. To get the better correlation between simulated and observed data, the multi-gauge calibration and validation of the model were carried out.

The observed streamflow data at various gauge stations of Krishna basin were collected from the Central Water Commission (GOI), Hyderabad and analysed. The variation of observed average monthly discharge in the Krishna river basin over a period of 31

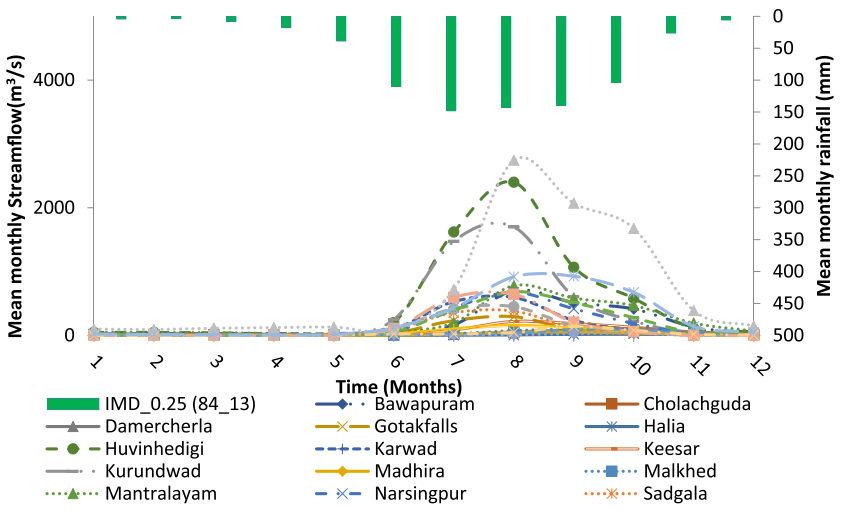

Fig. 3. Observed streamflow Vs Rainfall at different gauge stations located in Krishna river basin.

years (1984–2013) is shown in Fig. 3. The large streamflows occurred in July, August and September in Kurundwad and Huvinhedigi gauge stations were due to heavy rainfall in the Western Ghats in the months of June, July, August. As Vijayawada gauge station lies near the outlet of the Krishna basin, it receives heavy flows in months of July, August and September. The presence of reservoirs may cause the delay in the flows in this gauge station.

From the available streamflow data, the model was calibrated for a period of 22 years (1983–2004) and validated for a period of 8 years (2006–2013) at the gauge stations of Wadakbal, Wadenapally, Keesar, Yadgir, Matralayam and T. Ramapuram. Due to data limitation, at the gauge station of Malkhed, the calibration and validation periods were chosen as 1990–2007 and 2008–2013 respectively (Fig. 1). Sub-stream wise calibration was carried out. First, the model was calibrated at Wadkabal gauge station followed by Malkhed and Yadgir gauge stations. The model was then calibrated at T R Puram gauge station, followed by Mantralayam and Keesar gauge stations. Finally, the model was calibrated at Wadenapally, which is on the main stream of the Krishna river basin.

2.5. Selection criteria of climate model

The rainfall analysis of Krishna river basin was carried out using both, observed and historical climate model data of ten available climate models from CORDEX South-Asia data base. Compared mean ISMR of historical data of these ten models with observed data (IMD) based on their relative error, top six models (MIROC-MIROC5, NOAA-GFDL-GFDL-ESM2M, CNRM-CERFACS-CNRM-CM5, NCC-NorESM1-M, IPSL-CM5A-MR, and ICHES-EC-EARTH) were selected for further analysis (Fig. A1).

The use of RCMs driven by GCMs in regional studies is known as dynamic downscaling (Trzaska and Schnarr, 2014). The RCMs are able to represent atmospheric and landscape processes better than GCMs because of its higher resolutions. However, bias correction of these models is needed in regional studies (Brown et al., 2008) because of dynamical downscaling assumptions and caveats. Thus, distribution mapping bias correction method was used to reduce the uncertainty associated with the climate model data, as it can cope up with non-stationary conditions (Teutschbein et al., 2012). This method matches the distribution functions of observations and RCM simulated climate model values by correcting the distribution function of RCM simulated climate model values using transfer function.

Gamma distribution function (Eq. (1)) with shape factor (α) and scale factor (β) are used for the precipitation during bias correction. The shape factor (α) controls the profile distribution and scale factor (β) determines the dispersion of gamma distribution (Thom, 1958).

$$f_\gamma(x/\alpha, \beta) = x^{\alpha-1}\frac{1}{\beta^\alpha \Gamma(\alpha)} e^{-\left(\frac{x}{\beta}\right)}; \quad x \geq 0; \quad \alpha, \beta > 0 \tag{2}$$

The gaussian distribution (Cramér, 2016) with location parameter (μ) and scale parameter (α) is used for temperature time series (Eq. (2)). The detailed description of this method was given by Teutschbein and Seibert, 2012).

$$f_N(x|\ \mu, \sigma^2) = x^{\alpha-1}\frac{1}{\sigma\sqrt{2\Pi}} e^{-\frac{(x-\mu)^2}{2\sigma^2}}\ ;\ x€\mathscr{R} \tag{3}$$

During the months of June to October were selected for further analysis based on their contribution to total rainfall (86%). The model was selection based on the following criteria:

2.5.1. Taylor diagram

It is used to graphically quantify the similarity between two patterns (observed and modelled data) in terms of their correlation, centered root mean square difference (RMS), and amplitude of their variations (standard deviations) (Taylor, 2001). Statistics of six climate models were computed and the closeness of the model simulated rainfall and observed rainfall was seen (Fig. A2).

2.5.2. Statistical performance of the models

Statistical parameters such as the Root Mean Square Error (RMSE), Mean Error (ME), Mean Absolute Error (MAE), Mean Square Error (MSE), Correlation coefficient (r), Percent bias (PBIAS%), Standard deviation ratio (RSR), Kling-Gupta efficiency (KGE) and

Table 1
Comparison of statistical parameters of climate models (historical data) with observed rainfall (IMD) data (June to October).

Parameter	CNRM-CM5	GFDL-ESM-2M	ICHEC-ESM	MIROC-MIROC5	NorESM1M	IPSL-CM5A-MR
Relative error	0.066	0.146	0.094	0.065	**0.054**	0.22
ME	42.57	94.3	60.75	41.75	**35.11**	52.42
MAE	**159.3**	236.41	204.02	227.78	238.56	270
MSE	**57611.66**	98124.61	75903.45	91998.02	81922.91	136733
RMSE	**240.02**	313.25	275.51	303.31	286.22	369
PBIAS %	6.6	14.6	9.4	6.5	**5.4**	8.1
RSR	**1.24**	1.61	1.42	1.56	1.47	1.91
NSE	**−0.6**	−1.73	−1.11	−1.56	−1.28	−2.8
r	**0.18**	0.01	0.14	0	−0.18	−0.35
KGE	**0.17**	−0.02	0.12	−0.03	−0.18	−0.39

Relative error were used in the model selection as reported in Table 1.

2.5.3. Extreme event analysis

The five climate models were used to compare the historical rainfall data with observed data for the number of extreme events. The rainfall events were classified as:

Severe drought: Deficiency of ISMR more than 50%
Moderate drought: Deficiency of ISMR between 26–50%
Dry years: Deficiency of ISMR between 15–25%
Normal years: ISMR between + 15 to −15%
Wet years: Excess of ISMR between 15–25%
Excess rainfall: Excess of ISMR between 26–50%
Extreme rainfall: Excess of ISMR more than 50%

The 'extreme events' are defined as those events which come in the categories of severe drought, moderate drought, excess rainfall, and extreme rainfall.

3. Results and discussions

3.1. Climate model selection

The six climate models (ICHES-EC-EARTH; NOAA-GFDL-GFDL-ESM2M, MIROC-MIROC5, NCC-NorESM1-M, IPSL-CM5A-MR and CNRM-CERFACS-CNRM-CM5) projected the mean annual rainfall of historic climate data (1981–2005) to vary from 641 to 1022 mm, as against the observed rainfall value of 744 mm. Similarly, the mean ISMR (June to October) rainfall of the historic climate data was projected to be between 460–620 mm as against observed value of 647 mm. Hence, bias correction was adopted which reduced the projected mean annual rainfall to 787–853 mm and mean ISMR to 681–741 mm respectively, indicating a significant reduction in the model bias.

From the Taylor diagram, the model CNRM-CM5 showed a better statistical relationship with the observed data than the other models, as evident by the pattern correlation, centered root mean square (RMS) difference and standard deviation values of 0.179, 240, and 183 respectively (Fig. A2). In terms of statistical performance, CNRM-CM5 and NorESM-1 M models showed a better performance with the observed data in comparison to the other models (Table 1).

As far as the extreme events is concerned, the model CNRM-CM5 projected similar results as of the observed data (Table 2). From the above results, it was evident that the models CNRM-CM5 and NorESM1M gave closer predictions to the observed data. However, the model NorESM-1M was unable to capture the extreme events as observed. Therefore, the CNRM-CM5 climate model was selected for further analysis in this study. However, to understand the uncertainty in the projected future climate, multi-model projections were considered in this study.

3.2. Temperature analysis

The actual mean annual, maximum and minimum temperatures of 27, 32.97 and 21.06 °C respectively over Krishna basin (1984–2013) were closely projected by the CNRM-CM5 model as 27, 32.93 and 21.1 °C respectively after bias correction. Similarly, the actual mean monthly minimum and maximum temperatures of 15.65, and 38.96 °C respectively were closely projected by the CNRM-CM5 model as 15.53 and 39 °C.

The climate model (CNRM-CM5) projected an increasing trend in the mean monthly minimum and maximum temperatures of the Krishna river basin under future scenarios. An increase of 1.67 and 1.53 °C under RCP 4.5 scenario, and of 2.57 and 2.5 °C under RCP 8.5 scenario for the same was projected with reference to the baseline scenario, by the end of 21st century. The climate model also projected an increasing trend in the average annual temperature in both RCP 4.5 and 8.5 scenarios. An increase of 0.5, 1.05, 1.44 °C with reference to the baseline under RCP 4.5 scenario for the early, mid and end-centuries respectively. While RCP 8.5 scenario the increase was 0.61, 1.48, 2.6 °C respectively (Fig. 4).

Table 2
Number of extreme events (IMD vs Historical climate models data).

Event	IMD	CNRM-CM5	NorESM1M	GFDL-ESM2M	MIROC-MIROC5	ICHEC-ESM	IPSL-CM5A-MR
Normal Years	11	12	7	7	5	8	6
Dry Years	5	3	3	3	5	1	4
Moderate Drought	2	3	3	5	5	6	3
Severe Drought	0	0	1	0	1	0	2
Wet Years	2	2	4	5	0	4	1
Excess rainfall	1	1	4	2	5	3	5
Extreme Rainfall	1	1	0	0	1	2	1

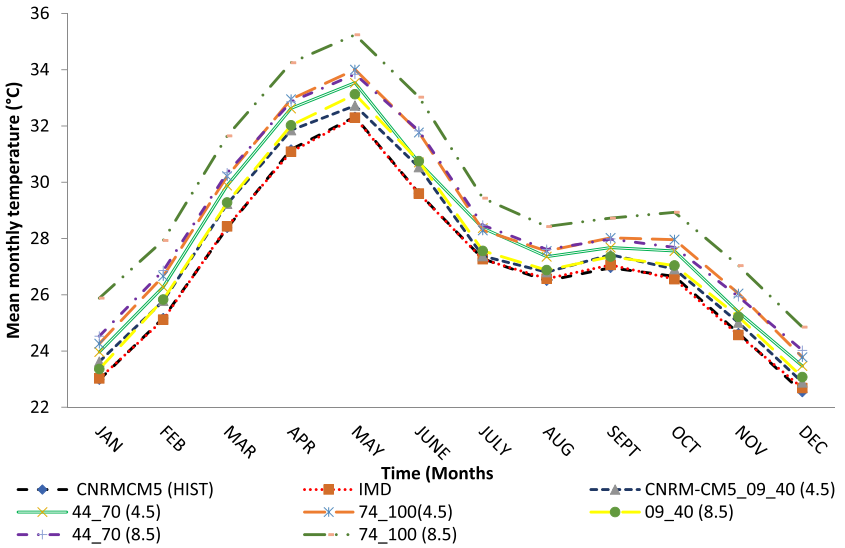

Fig. 4. Effect of climate change on mean monthly temperature under various future scenarios (CNRM-CM5 with RCP 4.5 and 8.5).

3.3. Calibration and Validation of the model

Sensitivity analysis was performed by using Latin hypercube and One factor at a time (LH-OAT) sampling methods (van Griensven and Meixner, 2006) in SWAT-CUP, to identify the sensitive parameters that can significantly influence the model output (Setegn et al., 2008). In this study, 15 were parameters were considered for the sensitivity analysis and the model was run for 1000 iterations at each gauge station during calibration. The larger absolute t-stat and lower p-value, indicate higher sensitivity. The t-stat identifies the relative significance, while p-value determines the significance of sensitivity. Based on sensitivity analysis, twelve parameters were identified as effective (CN2, RCHRG_DP, GWREVAP, SOL_K, GWDELAY, CH_K2, CH_N2, ALPHA_BNK, REVAPMN, ALPHA_BF,

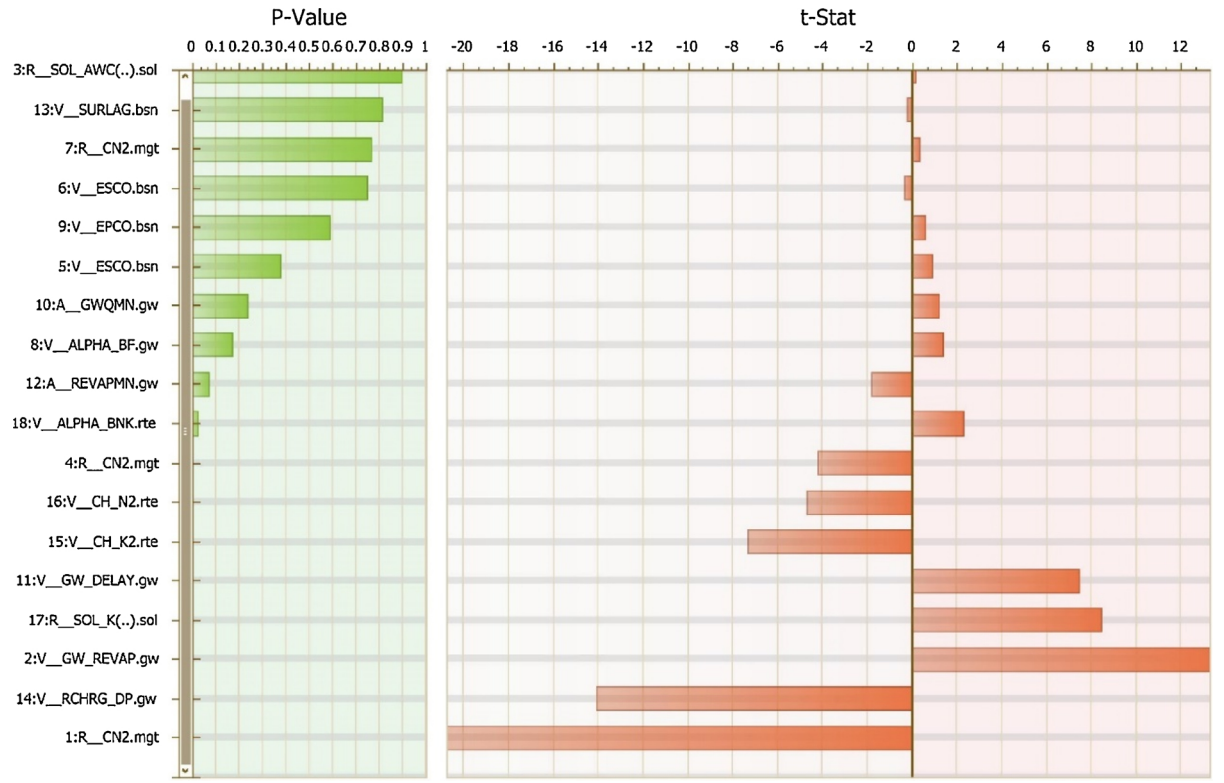

Fig. 5. Results of parameter sensitivity analysis (P-value and t-stat).

Table 3
Initial and final values of optimized parameters.

Parameter	Unit	State	LULC								
			CRDY	CRIR	CRGR	SHRB	SAVA	WATB	FOEB	FOEN	FODB	CRWO
CN		Initial	83.96	83.41	83.21	79.25	79.3	92	70	74	78.92	82
		Final	74.75	74.26	79	71.69	71.74	92	66.49	70.29	74.96	77.89
GWREVAP		Initial	0.02	0.02	0.02	0.02	0.02	0.02	0.02	0.02	0.02	0.02
		Final	0.186	0.186	0.192	0.186	0.186	0.186	0.186	0.186	0.186	0.186
ESCO		Initial	0.95	0.95	0.95	0.95	0.95	0.95	0.95	0.95	0.95	0.95
		Final	0.397	0.656	0.656	0.656	0.656	0.95	0.397	0.397	0.397	0.397
GWQMN	mm	initial	1000	1000	1000	1000	1000	1000	1000	1000	1000	1000
		Final	964.1	964.1	964.1	964.1	964.1	964.1	964.1	964.1	964.1	964.1
ALPHA_BF	days	initial	0.048	0.048	0.048	0.048	0.048	0.048	0.048	0.048	0.048	0.048
		Final	0.33	0.33	0.33	0.33	0.33	0.33	0.33	0.33	0.33	0.33
GW DELAY	days	initial	31	31	31	31	31	31	31	31	31	31
		Final	85.86	85.86	85.86	85.86	85.86	85.86	85.86	85.86	85.86	85.86
REVAPMN	mm	initial	750	750	750	750	750	750	750	750	750	750
		Final	819.6	819.6	819.6	819.6	819.6	819.6	819.6	819.6	819.6	819.6
RCHRG_DP		initial	0.05	0.05	0.05	0.05	0.05	0.05	0.05	0.05	0.05	0.05
		Final	0.044	0.044	0.044	0.044	0.044	0.044	0.044	0.044	0.044	0.044
SOL_K	mm/hr	initial	4.79	4.79	4.79	4.79	4.79	4.79	4.79	4.79	4.79	4.79
		Final	6.44	6.44	6.44	6.44	6.44	6.44	6.44	6.44	6.44	6.44

Note: CN2: SCS Curve Number II; GW_REVAP: Groundwater "revap" coefficient; ESCO: Soil Evaporation Compensation Factor; GWQMN: Threshold depth of water in the shallow aquifer required for return flow to occur; ALPHA_BF: Base flow alpha factor; GW_DELAY: Groundwater delay; RCHRG_DP: Deep aquifer percolation fraction; SOL_K: Saturated hydraulic conductivity; CH_N2: Manning's "n" value for main channel; CH_K2: Effective hydraulic conductivity in main channel alluvium; REVAPMN: Threshold depth of water in the shallow aquifer for "revap" to occur; ALPHA_BNK: Baseflow alpha factor for bank storage.

GWQMN, and ESCO) as shown in Fig. 5. The initial values of CH_K2, CH_N2, and ALPHA_BNK were 0, 0.014, and 0 and final values were 11.74, 0.082, and 0.26 respectively. Initial and final values of the other parameters corresponding to the particular land use/land cover types were shown in Table 3.

To evaluate the accuracy of the model, Coefficient of Regression (R^2) and Nash-Sutcliffe Efficiency (NSE) were used as objective functions. R^2 and NSE values greater than 0.5 indicate satisfactory results (Ghoraba, 2015; Liew et al., 2007). The R^2 and NSE values were found to vary from 0.6-0.8 and 0.58-0.79 respectively for calibration, and from 0.69-0.83 and 0.54-0.84 respectively for validation (Table 4), indicating satisfactory results in all the gauge stations. The influence of reservoirs and water storage structures were not considered, which may be a limitation of this study. It is also observed that the reservoirs were influencing the model calibration and validation results. The gauge stations which are free from the reservoirs (Malkhed and Keesar) has better results than other gauge stations which are influenced by reservoirs (Wadkbal, Yadgir, Mantralayam, T.R Puram and Wadenapalli). Even though the statistical values were found to be within permissible limits, the calibrated model was unable to capture a few peaks due to the detention and spilling of reservoirs at the gauge stations (Figs. 6 and 7).

The P-factor and R-factor are also used to quantify the model performance, the p-value closer to one and R-value closer to zero indicates the best fit. The P-factor represents the percentage of measured data bracketed by 95PPU, varies from zero to one. The R-factor is the ratio of average with of the band to the standard deviation of measured variables, varies from zero to infinity, the value of less than one is desirable (Abbaspour, 2013). The values of P-factor and R-factor in Table 4, indicates satisfactory results.

3.4. Analysis of water balance components under future scenarios

The water balance components (rainfall, surface runoff, evapotranspiration, and water yield) were quantified using SWAT model, with the exception of rainfall data which was sourced from IMD, India. Baseline scenario (historical climate data) was considered as

Table 4
Objective functions and their corresponding values.

Gauge station (Sub basin No)	Calibration		Validation		P-factor	R-factor
	R^2	NSE	R^2	NSE		
Wadkabal (18)	0.73	0.73	0.83	0.82	0.42	0.48
Malkhed (30)	0.8	0.79	0.9	0.84	0.9	0.73
Wadenapally (46)	0.6	0.58	0.69	0.6	0.61	0.83
Keesara (47)	0.78	0.76	0.76	0.71	0.84	0.97
Yadgir (63)	0.71	0.70	0.69	0.54	0.56	0.57
Mantralayam (102)	0.66	0.62	0.70	0.63	0.16	0.16
T. Ramapuram (116)	0.61	0.59	0.69	0.64	0.72	0.83

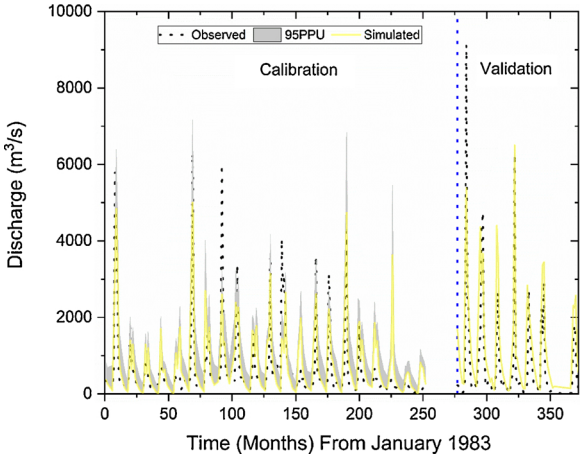

Fig. 6. Mean monthly observed Vs simulated streamflow of Wadenapally gauge station during calibration and validation (1983–2013).

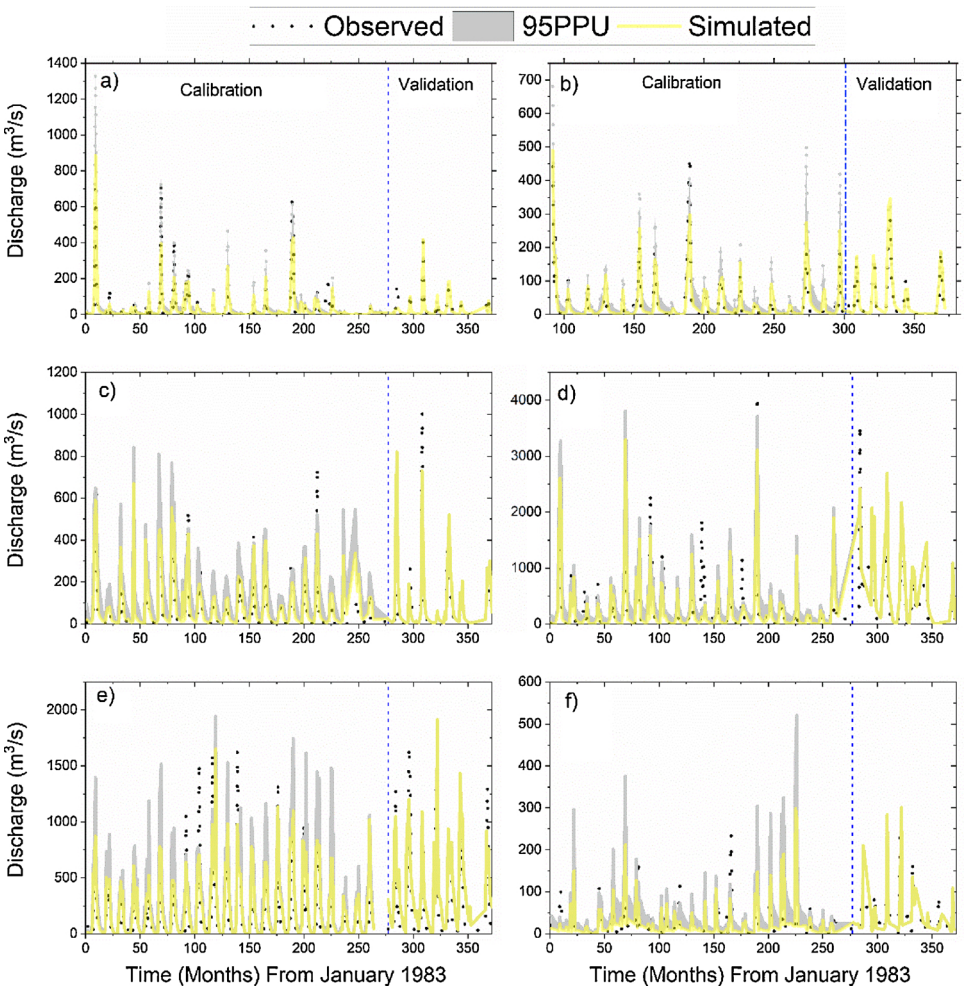

Fig. 7. Mean monthly observed Vs simulated streamflow of a) Wadakbal, b) Malkhed, c) Keesar d) Yadgir e) Mantralayam f) T. Ramapuram sub basins for the period (1983–2013).

the reference for evaluation of future scenarios.

The CNRM-CM5 model with RCP 4.5 scenario projected a 13, 7, and 2% decrease in the long-term mean ISMR rainfall in the early (2009–2040), mid (2044–2070), and end-centuries (2074–2100) respectively. This decreasing trend of rainfall was not uniform for

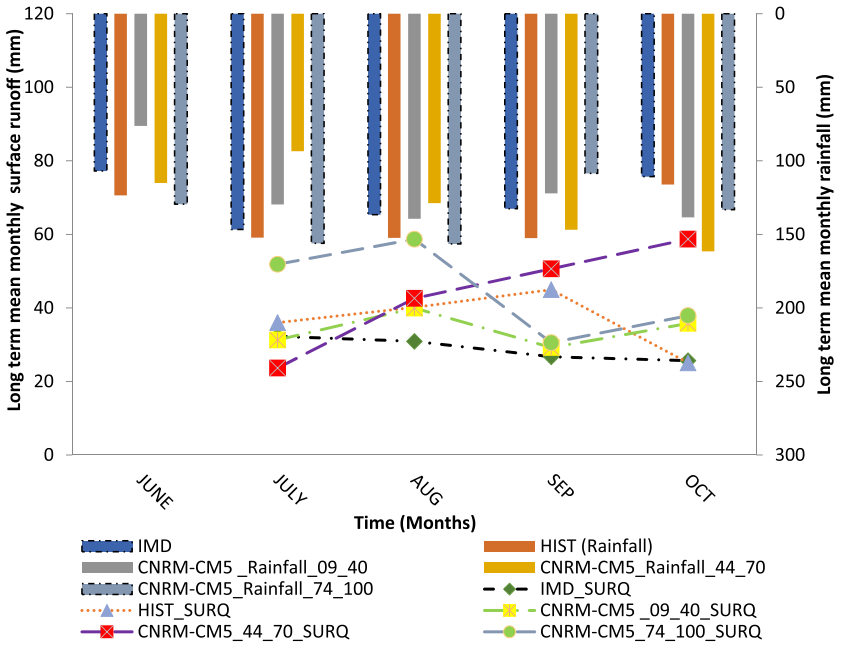

Fig. 8. Rainfall and surface runoff variations due to impact of climate change for different future scenarios (RCP 4.5).

the entire season. The long-term mean rainfall values for the months of June, July and September were projected to decrease by 47, 59, and 44 mm respectively for the early, mid, and end centuries. In contrast, rainfall in the month of October was projected to increase by 22, 45, and 17 mm respectively for the early, mid, and end centuries. While using RCP 8.5 scenario, the long-term mean ISMR was projected to decrease by 14% in the early century and increase by 6.5 and 22% for mid, and end centuries.

Overall, individual rainfall was found to decrease more than the mean for the months from June to September, whereas it was found to increase in the month of October (39 and 63 mm more than the mean for early and mid-centuries respectively). For the end century, rainfall in the month of September was projected to decrease by 38 mm from the mean, while it was projected to increase by 25 mm from the mean, for the month of October. An increasing trend of rainfall was projected for the month of November throughout the early, mid, and end centuries (RCP 4.5 and 8.5), indicating that the variation of rainfall under future scenarios was non-uniform, varying on a monthly basis.

An increase in rainfall for the months of October and November and a shift in the occurrence of maximum surface runoff were the key projections from the model run. While the maximum surface runoff was observed in the month of September as per the baseline scenario, it was projected to occur in the month of August for the early and end centuries, and in October for the mid-century as per RCP 4.5 scenario. RCP 8.5 scenario projected the maximum surface runoff to occur in the months of August, October, and June months for early, mid, and end centuries respectively (Figs. 8 and 9). The shift in the occurrence of the maximum surface runoff can be attributed mainly due to the changes in the temporal variation of rainfall over the basin. The timing and strength of monsoon depend mainly on the land-sea thermal contrast, which in-turn affects the atmospheric moisture content. Indian sub-continent sea surface temperature increased more rapidly than the land surface temperature, thus reducing the land-sea thermal contrast, hence weakening the monsoon rainfall (Mishra et al., 2012; Rajeevan et al., 2008; Roxy, 2017). This leads to a change in the atmospheric moisture content, along with the timing and magnitude of rainfall over the region, leading to early onset dates and delayed retreating days. The lengthening of Indian monsoon rainfall may be the reason behind the increasing rainfall in the months of October and November, resulting in a decrease in rainfall in the monsoon season, and a shift in maximum surface runoff under future scenarios. These results indicate a varibility of rainfall and streamflow over the basin, under future scenarios.

In this study, water balance components such as the mean surface runoff, water yield, and ET were projected to decrease by 6.8, 11, and 9% respectively from the baseline (under RCP 4.5 scenario), and by 4.8, 9.6, and 11.5% respectively (under RCP 8.5 scenario) for the early century. For the mid-century (2044–2070), the surface runoff and water yield were projected to increase by 20 and 6.8% respectively under RCP 4.5 scenario, and by 39 and 29% respectively under 8.5 scenario. No variations were projected for the ET by RCP 4.5 scenario, but a 1% increase was projected in the same, using RCP 8.5 scenario. For the end-century, the mean surface runoff, water yield, and ET were projected to increase by 64.6, 56.2, and 11.6% using RCP 8.5 scenario, and by 22.4, 10 and 7.3% under RCP 4.5 scenario (Table 5). These results indicate that the surface runoff and water yield were more sensitive to climate change (i.e., changes in rainfall) than evapotranspiration.

Mishra and Lilhare (2016) projected a contionous increasing trend of water balance components along with rainfall and air temperature in both RCP 4.5 and 8.5 scenarios of CMIP5 models in the Krishna river basin. Rainfall increase of about 8–20% under RCP 4.5 and 10–40% in the case of RCP 8.5 by the end century. Similarly, the surface runoff, streamflow and ET were projected increase of about 20–55%, 20–60% and 4–9% under RCP 4.5 and 35–120%, 40–120% and 2–8% in case RCP 8.5 by the end century.

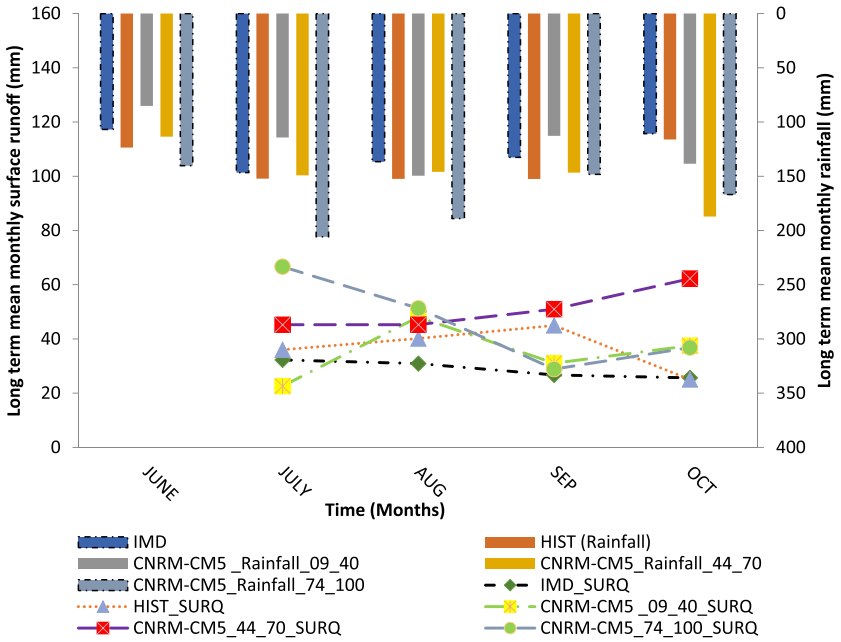

Fig. 9. Rainfall and surface runoff variations due to impact of climate change for different future scenarios (RCP 8.5).

Table 5
Hydrological variables of ISMR of Krishna basin for RCP 4.5 & 8.5 (CNRM-CM5).

Scenario	Rainfall (mm)	Surface runoff (mm)	Water yield (mm)	Evapotranspiration (mm)
IMD (1984-05)	634	116	133	334
Historic (1984-05)	697(63)	146 (30)	178(45)	297(−37)
Early century, RCP 4.5 (2009-2040)	606 (−13%)	136 (-6.8%)	159(−11%)	269 (−9.2%)
Mid-century, RCP 4.5 (2043-2070)	646 (−7%)	176 (20%)	190(6.8%)	294 (-1%)
End century, RCP 4.5(2073-2100)	684 (−2%)	179 (22.4%)	196(10%)	318 (7.3%)
Early century, RCP 8.5 (2009-2040)	600 (−14%)	139 (−4.8%)	161(-9.6%)	263 (−11.5%)
Mid-century, RCP 8.5 (2043-2070)	743 (6.5%)	204 (39.3%)	230 (29%)	298 (0.2%)
End century, RCP 8.5(2073-2100)	850 (22%)	241 (64.6%)	279 (56.2%)	331 (12%)

Note: (): % deviation observed from long-term historical average; -ve: deficit; +ve: excess.

Table 6
Number of extreme events projected for future scenarios CNRM-CM5-RCP 4.5 (8.5).

Event	IMD (1984–2005)	Historical (1984–2005)	2018–2040	2044–2070	2074–2100
Normal Years	11	12	12 (7)	10 (13)	9 (10)
Dry Years	5	3	4 (4)	2 (3)	6 (1)
Moderate Drought	2	3	4 (9)	9 (3)	6 (1)
Severe Drought	0	0	0 (1)	0 (0)	0 (0)
Wet Years	2	2	1 (0)	3 (2)	2 (3)
Excess Rainfall	1	1	0 (1)	2 (3)	3 (8)
Extreme Rainfall	1	1	2 (1)	1(3)	1(4)

3.5. Analysis of extreme events under future scenarios (CNRM-CM5)

The hydrological regimes of the Krishna river basin was found to be sensitive to climate change. The maximum and minimum ISMR over the Krishna basin were 1440 mm and 360 mm respectively under RCP 4.5 scenario, and 1353 mm and 320 mm for RCP 8.5

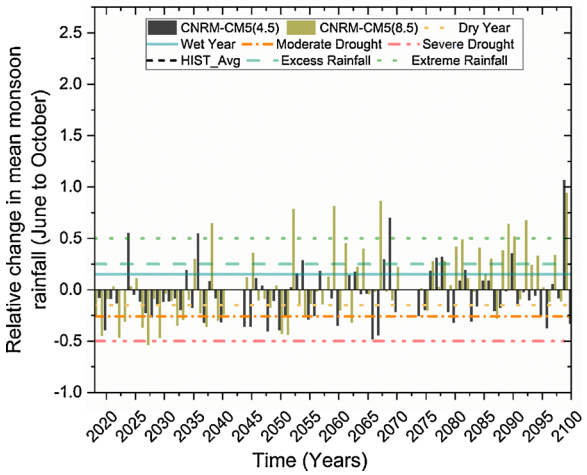

Fig. 10. Relative change in mean monsoon rainfall due to extreme events under future scenarios (CNRM-CM5).

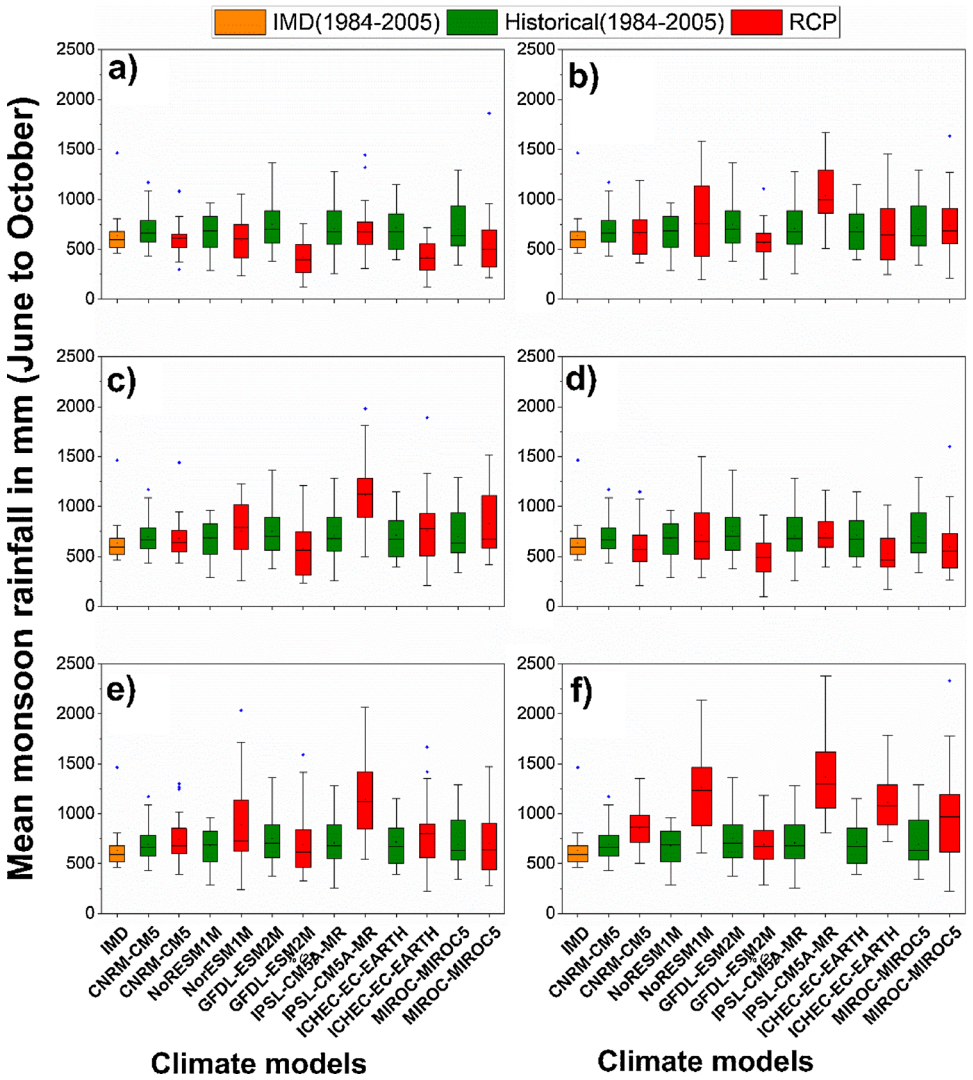

Fig. 11. Comparison of mean monsoon rainfall under different climate model with reference to historical data.

Table 7
Uncertainty range of hydrological variables of ISMR (June to October) of Krishna basin.

Scenario	Rainfall (mm)	Surface runoff (mm)	Water yield (mm)	Evapotranspiration (mm)
IMD (1984-05)	634	116	133	334
Historic (1984-05)	704 (693–739)	150.6 (110–175)	185.7 (166–206)	317 (297–329)
Early century, RCP 4.5 (2009-2040)	544 (422–677)	129 (88–176)	143 (95–202)	255 (203–314)
Mid-century, RCP 4.5 (2044-2070)	739 (566–1029)	241 (173–386)	262 (180–430)	295 (244–319)
End century, RCP 4.5(2074-2100)	784 (578–1112)	278 (179–484)	310 (196 -528)	307 (257–383) (307)
Early century, RCP 8.5 (2009-2040)	611 (501–734)	160 (125–202)	175 (133–228)	271 (226–300)
Mid-century, RCP 8.5 (2044-2070)	828 (689–1147)	275 (198- 462)	302 (221–510)	308 (274–394)
End century, RCP 8.5(2074-2100)	1038 (696–1360)	409 (236–622)	454 (256–694)	339 (278–415)

Note: The values in () indicates prediction bounds of climate models (MIROC-MIROC5, GFDL-ESM2M, ICHEC-ESM, IPSL-CM5A, NorESM1M and CNRM-CM5).

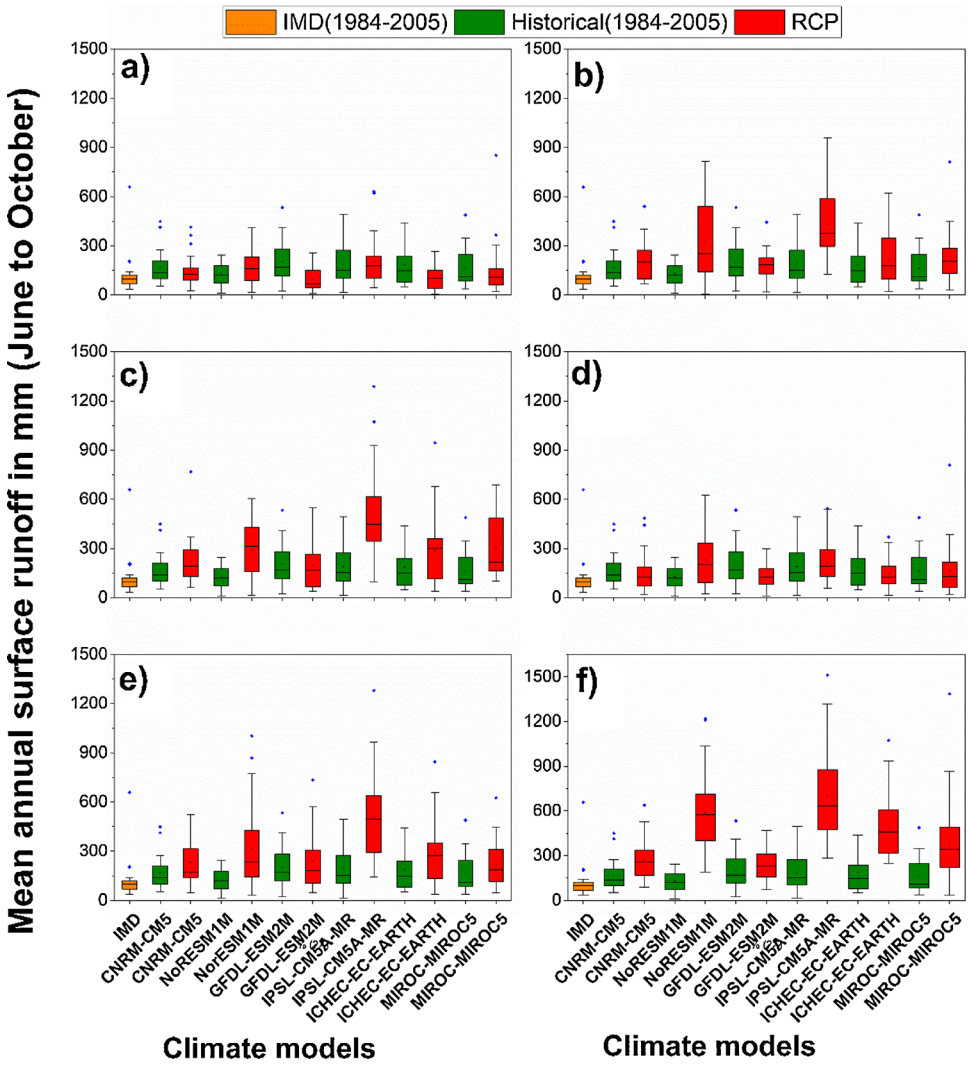

Fig. 12. Comparison of mean monsoon surface runoff under different climate model with reference to historical data.

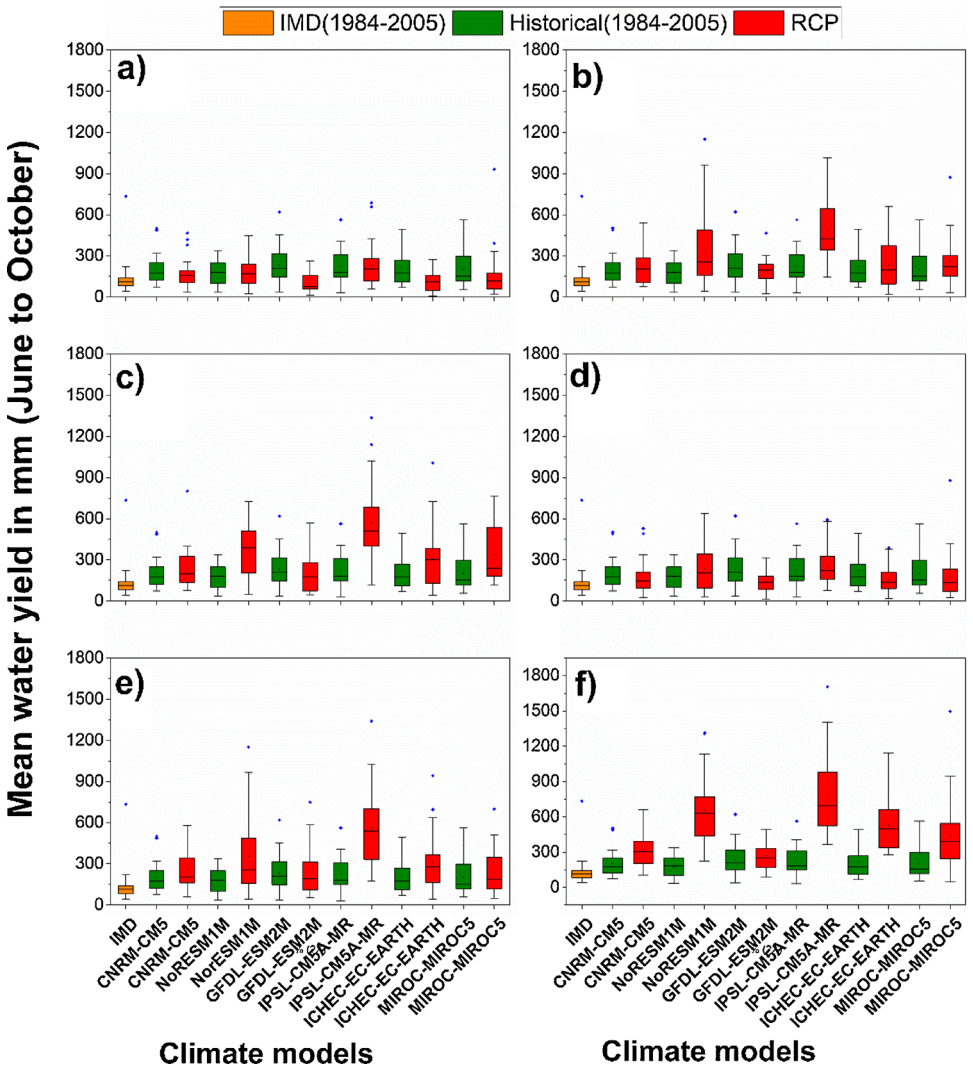

Fig. 13. Comparison of mean monsoon water yield under different climate model with reference to historical data.

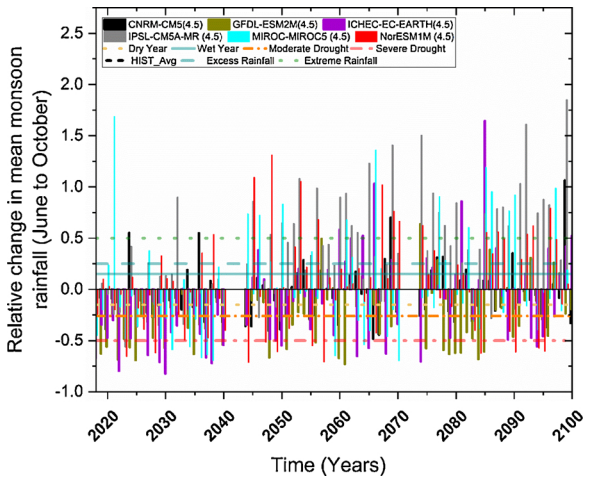

Fig. 14. Relative change in mean projected rainfall of climate models with respective to historical mean under RCP 4.5 scenario.

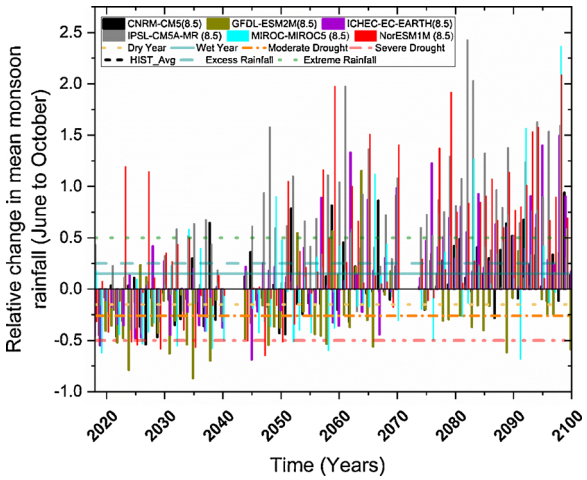

Fig. 15. Relative change in mean projected rainfall of climate models with respective to historical mean under RCP 8.5 scenario.

scenario respectively (Fig. A3). The number of extreme events in both, observed and historical data (CNRM-CM5) were almost similar to the early century predictions under RCP 4.5 scenario. However, in the mid and end centuries, the number of normal years followed a decreasing trend, and the extreme events (especially moderate drought) followed an increasing trend. Prediction using RCP 8.5 scenario showed different trends for each timeline. In the early century, the number of normal years was projected to decrease, and the extreme events (especially moderate drought) were projected to increase.

40% of the years in the early century were projected to be moderate drought years under RCP 8.5 scenario. A severe drought (in the year 2027) was also projected in the early century. The mid century predictions followed a different scenario than that of the early century. The number of normal years projected were almost similar to the historical data, but the number of excess and extreme rainfall events were projected to increase. The end century predictions revealed that excess and extreme rainfall events comprise 45% of the years (Table 6). RCP 8.5 scenario projected the occurrence of continuous excess and extreme rainfall events between 2088–2094 (Fig. 10), attributed to an increasing atmospheric humidity and saturation water vapor pressure under a warmer climate. It was evident that irrespective of the scenario, there were significant changes in the extreme events in the future.

3.6. Multi-model projections

Multi-model projections were used to understand the uncertainties in the projected future climate. The relative change between observed (IMD) and historical climate models rainfall projections were between 8–17% (Fig. 11). The CNRM-CM5 projections were closer to the mean of six climate models except in the end century (Table 7). In the early century, all models projected a decrease in rainfall and water balance components except IPSL-CM5A-MR and NorESM-1 M (Fig. 11(a) and (b)) with respective to their long-term historical mean. Whereas in mid and end centuries the projections are vary with the models (Fig. 11). The uncertainty range of these climate models are between GFDL-ESM-2 M and IPSL-CM5A-MR projections. The GFDL-ESM2M projected a decrease in rainfall under future scenarios, while IPSL-CM5A-MR projected an increase of rainfall (Fig. 11). The Figs. 12 and 13 shows the changes in projected mean, minimum and maximum (along with outliers) values of surface runoff and water yield for climate models with reference to historical data.

3.6.1. Extreme events under multi-model projections

The maximum and minimum ISMR (June to October) over the Krishna basin were 1981 mm with IPSL-CM5A-MR in 2099 and 124 mm with ICHEC-EC-EARTH in 2030 respectively under RCP 4.5 scenario (Fig. A4), whereas RCP 8.5 scenario projected maximum of 2382 mm with IPSL-CM5A-MR in 2082 and minimum of 96 mm with GFDL-ESM-2 M in 2035 (Fig. A5). The extreme events projected to increase in future scenarios. The early century projected an increase of drought events due to a decrease of mean ISMR in both RCP 4.5 and 8.5 scearios, whereas an increase of wet events was projected in mid and end centuries. Especially the extreme rainfall events were projected to increse in end century under RCP 8.5, while in case of RCP 4.5, the drought and extreme rainfall events are likely to occur in equal probability (Figs. 14 and 15).

The maximum and minimum water yield (June to October) over the Krishna basin was 1336 mm with IPSL-CM5A-MR in 2099 and 7 mm with NorESM-1 M in 2044 respectively under RCP 4.5 scenario (Fig. A6), whereas RCP 8.5 scenario projected maximum of 1705 mm with IPSL-CM5A-MR in 2082 and minimum of 14 mm with GFDL-ESM-2 M in 2035 (Fig. A7). The mean water yield projected to decrese in early century in both RCP 4.5 and 8.5 scearios. While in case of mid and end centuries, the mean water yield was projected to increase. There is an increase in the mean of about 1.5 times to the long term mean historical water yield by the end century under RCP 8.5 (Figs. A6 and A7).

4. Conclusions

In this study, water balance components such as surface runoff, water yield and evapotranspiration were simulated under future climate scenarios using both RCP 4.5 and 8.5 scenarios. The climate model (CNRM-CM5) projected a decreasing trend of rainfall under RCP 4.5 scenario, whereas under RCP 8.5 scenario, it predicts a decrease of rainfall in early century and increasing trend for the mid and end centuries. For an early century, the rainfall, surface runoff, water yield and ET were followed a decreasing trend in both the scenarios (RCP 4.5 and 8.5). For the mid-century, the surface runoff and water yield were projected to increase under 4.5 and 8.5 scenario. No variations were projected for the ET by RCP 4.5 scenario, but a slight increase was projected in the same, using RCP 8.5 scenario. For the end-century, the mean annual surface runoff, water yield and ET were projected to increase in both RCP 4.5 and 8.5 scenarios.

The extension of monsoon rainfall even up to October, shift in the occurrence of the maximum amount of long-term mean ISMR and maximum surface runoff along with an increasing trend of rainfall in the months of October and November were the key projections from the model run. The increase in rainfall in the months of October - November has adverse impact on kharif crops as it is a crop harvesting stage. The climate model projected a few extreme rainfall events in a non-monsoon season and also, the frequencies of extreme weather events are more under the future climate scenarios. Finally, siginificent changes were projected in the extreme events in all the scenarios. In consideration of future projected climate changes, it was necessary to change water management strategies in the basin for sustainable planning and management of water resources. Rainwater harvesting systems have to be implimented to tap the surplus runoff in the respective months and to supply for the need of demand because these months were crucial for Kharif crops. Further, the results may improve by including the effect of reservoirs and dynamic land changes on the basin.

Conflicts of interest

The authors declare no conflict of interest.

Acknowledgments

The authors like to acknowledge the support from Frontier Areas of Science and Technology - Centre of Excellence (FAST-CoE) in Sustainable Development at I.I.T. Hyderabad, funded by the Ministry of Human Resource Development, India. The authors also like to acknowledge the Indian Meteorological Department (IMD) and Central Water Commission (CWC), Hyderabad for their support in sharing the data and also thanks to Earth System Grid Federation (ESGF) for their (climate model) data support. The open access publishing fees for this article have been partially covered by the Texas A&M University Open Access to Knowledge Fund (OAK Fund), supported by the University Libraries and the Office of the Vice President for Research.

Appendix A

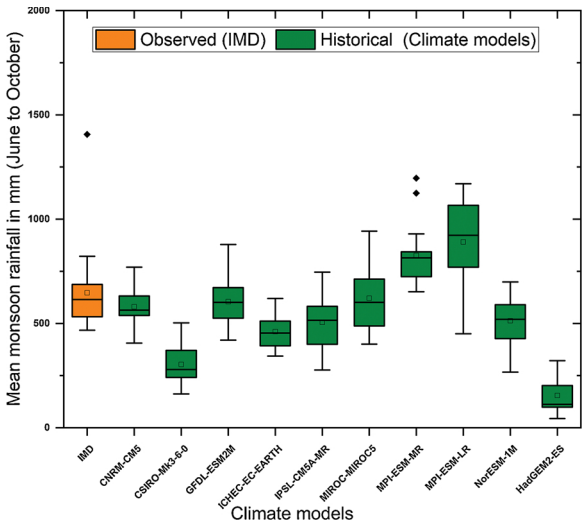

Fig. A1. Comparison of mean historical and observed (ISMR) rainfall data (before bias correction).

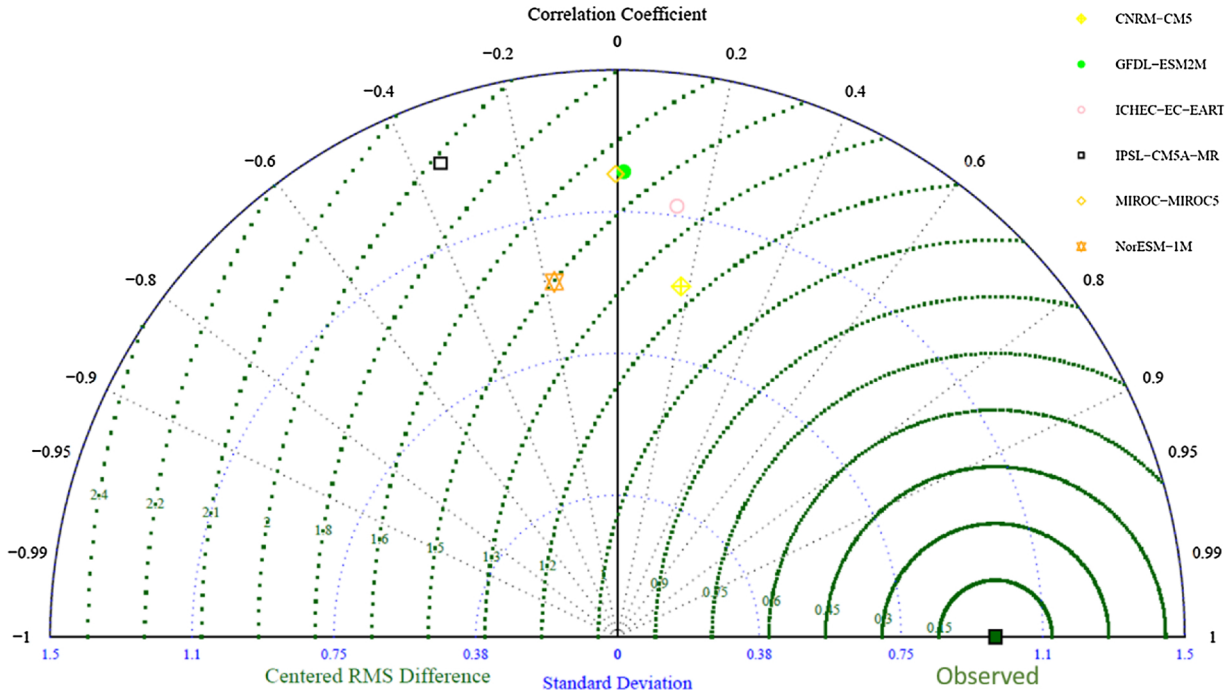

Fig. A2. Taylor diagram of climate models with observations.

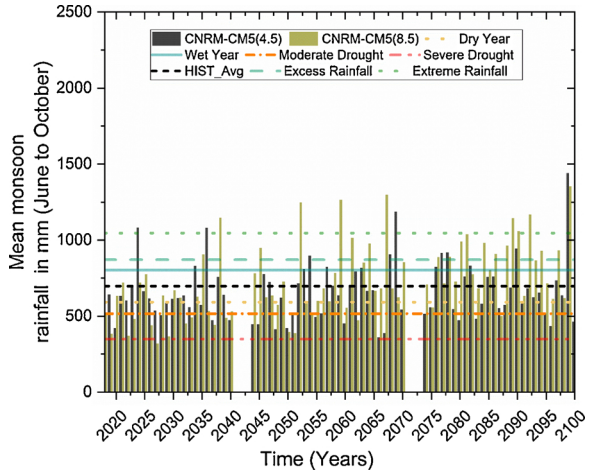

Fig. A3. Extreme rainfall events under CNRM-CM5.

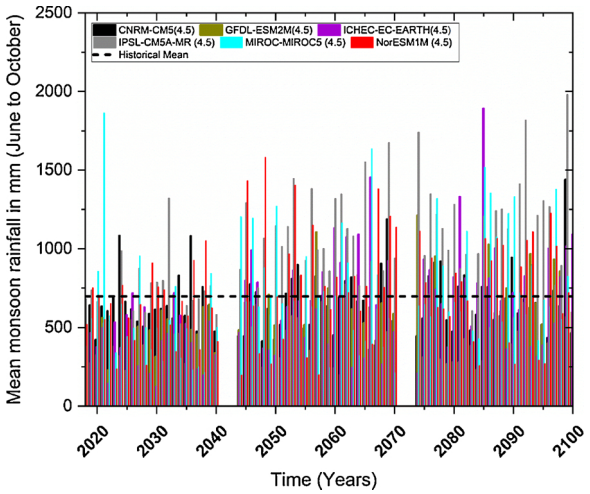

Fig. A4. Extreme rainfall events under multi-model projections (RCP 4.5).

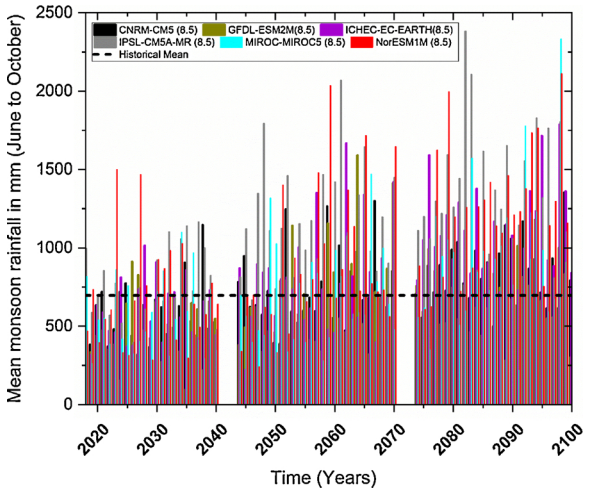

Fig. A5. Extreme rainfall events under multi-model projections (RCP 8.5).

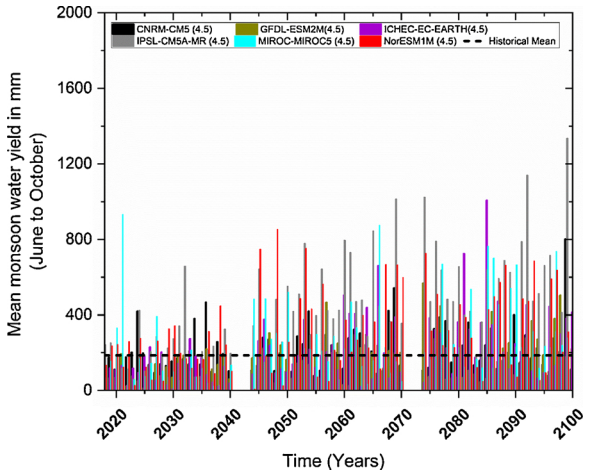

Fig. A6. Mean water yield under multi-model projections (RCP 4.5).

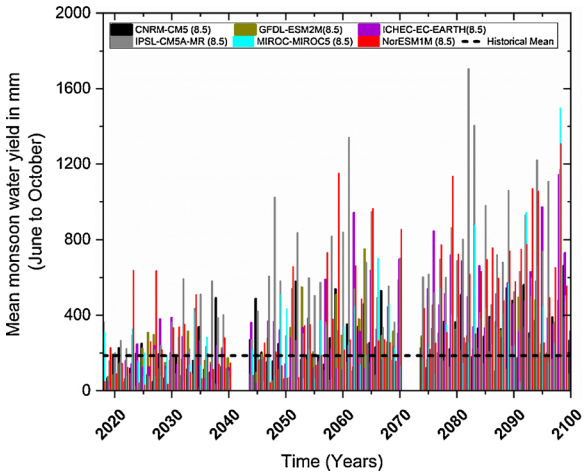

Fig. A7. Mean water yield under multi-model projections (RCP 8.5).

References

Abbaspour, K.C., 2013. SWAT-CUP 2012: SWAT Calibration and Uncertainty Programs–a User Manual. Eawag, Dübendorf, Switzerland, pp. 103.

Abbaspour, K.C., Rouholahnejad, E., Vaghefi, S., Srinivasan, R., Yang, H., Kløve, B., 2015. A continental-scale hydrology and water quality model for Europe: calibration and uncertainty of a high-resolution large-scale SWAT model. J. Hydrol. 524, 733–752 Elsevier B.V.

Arnell, N.W., Reynard, N.S., 1996. The effects of climate change due to global warming on river flows in Great Britain. J. Hydrol. 183, 397–424.

Arnold, J.G., Srinivasan, R., Muttiah, R.S., Williams, J.R., 1998. Large area hydrologic modeling and assessment part I: model development. JAWRA J. Am. Water Resour. Assoc. 34 (1), 73–89.

Brown, C., Greene, A., Block, P., Giannini, A., 2008. Review of Downscaling Methodologies for Africa Climate Applications. International Research Institute for Climate and Society. Columbia University.

Cramér, H., 2016. Mathematical Methods of Statistics (PMS-9), vol. 9 Princeton University Press.

Devkota, L.P., Gyawali, D.R., 2015. Impacts of climate change on hydrological regime and water resources management of the Koshi River Basin, Nepal. J. Hydrol. Reg. Stud. 4, 502–515 Elsevier B.V.

Easterling, D.R., Meehl, G.A., Parmesan, C., Changnon, S.A., Karl, T.R., Mearns, L.O., 2000. Climate extremes: observations, modeling, and impacts. Science 289 (5487), 2068–2074.

Fujihara, Y., Tanaka, K., Watanabe, T., Nagano, T., Kojiri, T., 2008. Assessing the impacts of climate change on the water resources of the Seyhan River Basin in Turkey: use of dynamically downscaled data for hydrologic simulations. J. Hydrol. 353 (1–2), 33–48.

Ghoraba, S.M., 2015. Hydrological modeling of the Simly Dam watershed (Pakistan) using GIS and SWAT model. Alexandria Eng. J. 54 (3), 583–594 Faculty of Engineering, Alexandria University.

Gosain, A.K., Rao, S., Arora, A., 2011. Climate change impact assessment of water resources of India. Curr. Sci. 101 (3), 356–371.

Gosain, A.K., Rao, S., Basuray, D., 2006. Climate change impact assessment on hydrology of Indian river basins. Curr. Sci. 346–353.

Gumma, M.K., Thenkabail, P.S., Nelson, A., 2011. Mapping irrigated areas using MODIS 250-meter time-series data: a study on Krishna River Basin (India). Water 3 (1), 113–131.

Guo, S., Wang, J., Xiong, L., Ying, A., Li, D., 2002. A macro-scale and semi-distributed monthly water balance model to predict climate change impacts in China. J. Hydrol. 268 (1–4), 1–15.

Iskender, I., Sajikumar, N., 2016. Evaluation of surface runoff estimation in ungauged watersheds using SWAT and GIUH. Procedia Technol. 24, 109–115 Elsevier B.V.

Jiang, Tao, David Chen, Yongqin, Xu, Chong-yu, Chen, Xiaohong, Chen, Xi, Singh, Vijay P., 2007. Comparison of hydrological impacts of climate change simulated by six hydrological models in the Dongjiang Basin, South China. J. Hydrol. 336, 316–333.

Karl, T.R., 2008. Weather and Climate Extremes in a Changing Climate.

Kulkarni, B.D., Deshpande, N.R., Patwardhan, S.K., Bansod, S.D., 2014. Assessing hydrological response to changing climate in the Krishna Basin of India. J. Earth Sci. Clim. Change 5 (7), 6.

Liew, M.W. Van, Veith, T.L., Bosch, D.D., Arnold, J.G., 2007. Suitability of SWAT for the Conservation Effects Assessment Project: Comparison on USDA Agricultural Research Service Watersheds. J. Hydrol. Eng. 12 (2), 173–189.

Mishra, N., Aggarwal, S.P., Dadhwal, V.K., 2008. Macroscale Hydrological Modelling and Impact of land cover change on stream flows of the Mahanadi River Basin. A Master thesis submitted to Andhra University, Indian Institute of Remote Sensing (National Remote Sensing Agency) Dept. of Space, Govt. of India.

Mishra, V., Lilhare, R., 2016. Hydrologic sensitivity of Indian sub-continental river basins to climate change. Glob. Planet. Change 139, 78–96.

Mishra, V., Smoliak, B.V., Lettenmaier, D.P., Wallace, J.M., 2012. A prominent pattern of year-to-year variability in Indian Summer Monsoon Rainfall. Proc. Natl. Acad. Sci. 109 (19), 7213–7217.

Mishra, V., Kumar, D., Ganguly, A.R., Sanjay, J., Mujumdar, M., Krishnan, R., Shah, R.D., 2014. Reliability of regional and global climate models to simulate precipitation extremes over India. J. Geophys. Res. Atmos. 119 (15), 9301–9323.

Mishra, V., Aadhar, S., Asoka, A., Pai, S., Kumar, R., 2016. On the frequency of the 2015 monsoon season drought in the Indo-Gangetic Plain. Geophys. Res. Lett. 43 (23).

Molina-Navarro, E., Hallack-Alegría, M., Martínez-Pérez, S., Ramírez-Hernández, J., Mungaray-Moctezuma, A., Sastre-Merlín, A., 2016. Hydrological modeling and climate change impacts in an agricultural semiarid region. Case study: guadalupe River basin, Mexico. Agric. Water Manag. 175, 29–42 Elsevier B.V.

Mukherjee, S., Aadhar, S., Stone, D., Mishra, V., 2018. Increase in extreme precipitation events under anthropogenic warming in India. Weather Clim. Extrem.

Neitsch, S.L., Arnold, J.G., Kiniry, J.R., Williams, J.R., 2011. Soil and Water Assessment Tool Theoretical Documentation Version 2009. Water Resources Institute, Texas.

NRAA, 2011. Impact of High Rainfall/Floods on Ground Water Resources in the Krishna River Basin (during 1999-2009). Study Report 2. National Rainfed Area Authority, New Delhi, India 92 p.

Pai, D.S., Sridhar, L., Rajeevan, M., Sreejith, O.P., Satbhai, N.S., Mukhopadhyay, B., 2014. Development of a new high spatial resolution (0.25× 0.25) long period (1901–2010) daily gridded rainfall data set over India and its comparison with existing data sets over the region. Mausam 65 (1), 1–18.

Prajnya, V.H., Tuppad, P., 2016. Study of hydrologic response of kabini basin using soil and water assessment tool (SWAT). Int. J. Eng. Sci. 6 (8), 2373–2380.

Rajeevan, M., Bhate, J., Jaswal, A.K., 2008. Analysis of variability and trends of extreme rainfall events over India using 104 years of gridded daily rainfall data. Geophys. Res. Lett. 35 (18).

Roxy, M.K., 2017. Climate dynamics: land warming revives monsoon. Nat. Clim. Chang. 7 (8), 549.

Setegn, S.G., Srinivasan, R., Dargahi, B., 2008. Hydrological Modelling in the Lake Tana Basin, Ethiopia Using SWAT Model. Open Hydrol. J. 2 (1), 49–62.

Shrestha, S., Htut, A.Y., 2016. Modelling the potential impacts of climate change on hydrology of the Bago River Basin, Myanmar. Int. J. River Basin Manag. 14 (3), 287–297.

Singh, A., Gosain, A.K., 2012. GIS based hydrological modelling for climate change impact assessment. Greener J. Sci., Eng. Technol. Res. 3 (7), 210–219.
Soro, G.E., Yao, A.B., Kouame, Y.M., Bi, T.A.G., 2017. Climate change and its impacts on water resources in the Bandama Basin, Côte D'ivoire. Hydrology 4 (1), 18.
Taylor, K.E., 2001. Summarizing multiple aspects of model performance in a single diagram. J. Geophys. Res. Atmos. 106 (D7), 7183–7192.
Teutschbein, C., Seibert, J., 2012. Bias correction of regional climate model simulations for hydrological climate-change impact studies: review and evaluation of different methods. J. Hydrol. 456, 12–29.
Thom, H.C., 1958. A note on the gamma distribution. Mon. Weather. Rev. 86 (4), 117–122.
Thomson, A.M., Calvin, K.V., Smith, S.J., Kyle, G.P., Volke, A., Patel, P., Delgado-arias, S., Bond-lamberty, B., Wise, M.A., Clarke, L.E., Edmonds, J.A., 2011. RCP4. 5: a pathway for stabilization of radiative forcing by 2100. Clim. Change 109 (1-2), 77–94.
Trzaska, S., Schnarr, E., 2014. A Review of Downscaling Methods for Climate Change Projections. United States Agency for International Development by Tetra Tech ARD, pp. 1–42.
van Griensven, A., Meixner, T., 2006. Methods to quantify and identify the sources of uncertainty for river basin water quality models. Water Sci. Technol. 53 (1), 51–59.
Vu, M.T., Raghavan, S.V., Liong, S.Y., 2016. Use of regional climate models for proxy data over transboundary regions. J. Hydrol. Eng. 21 (6), 1–10.
Yang, J., Reichert, P., Abbaspour, K.C., Xia, J., Yang, H., 2008. Comparing uncertainty analysis techniques for a SWAT application to the Chaohe Basin in China. J. Hydrol. 358 (1–2), 1–23.
Zhang, D., Chen, X., Yao, H., Lin, B., 2015. Improved calibration scheme of SWAT by separating wet and dry seasons. Ecol. Modell. 301, 54–61 Elsevier B.V.
Zhang, G.H., Nearing, M.A., Liu, B.Y., 2006. Potential effects of climate change on rainfall eosivity in the Yellow River Basin of China. Trans. ASAE 48 (2), 511–517.
Zierl, B., Bugmann, H., 2005. Global change impacts on hydrological processes in Alpine catchments. Water Resour. Res. 41 (2), 1–13.